Hindawi Publishing Corporation
Journal of Nanomaterials
Volume 2013, Article ID 587021, 10 pages
http://dx.doi.org/10.1155/2013/587021

Research Article

Iron Oxide Magnetic Nanoparticles: Characterization and Toxicity Evaluation by *In Vitro* and *In Vivo* Assays

Alina Mihaela Prodan,[1,2] Simona Liliana Iconaru,[3] Carmen Steluta Ciobanu,[3] Mariana Carmen Chifiriuc,[4] Mihai Stoicea,[2] and Daniela Predoi[3]

[1] *Carol Davila University of Medicine and Pharmacy, 8 Eroii Sanitari, Sector 5, 050474 Bucharest, Romania*
[2] *Emergency Hospital Floreasca, Bucharest 5, Calea Floreasca Nr 8, Sector 1, 014461 Bucarest, Romania*
[3] *National Institute of Materials Physics, 105 bis Atomistilor, P.O. Box MG 07, 077125 Bucuresti-Magurele, Romania*
[4] *Microbiology Department, Faculty of Biology, University of Bucharest, Aleea Portocalelor 1-3, 60101 Bucharest, Romania*

Correspondence should be addressed to Daniela Predoi; dpredoi@gmail.com

Received 21 August 2013; Revised 4 October 2013; Accepted 5 October 2013

Academic Editor: In-Kyu Park

The aim of this study was to evaluate the biological properties of iron oxide nanoparticles (IO-NPs) obtained in the aqueous suspension. The iron oxide nanoparticles were characterized by scanning electron microscopy (SEM) and transmission electron microscopy (TEM). The biocompatibility of the iron oxide was demonstrated by the *in vitro* quantification of HeLa cells viability using propidium iodide (PI) and fluorescein diacetate (FdA) and the MTT colorimetric assay. The toxicity of small size iron oxide nanoparticles was also evaluated by means of histological examination on male Brown Norway rats after intraperitoneal injection. At the tested concentrations, the nanoparticles proved to be not cytotoxic on HeLa cells. The rat's behavior, as well as the histopathological aspect of liver, kidney, lung, and spleen tissues at 48 h after intraperitoneal injection did not present any modifications. The *in vivo* and *in vitro* assays suggested that the IO-NPs could be further used for developing new *in vivo* medical applications.

1. Introduction

Nowadays, finding new approaches for solving pressing problems in the field of medical science is the focus of research institutes everywhere. The most studied materials with promising potential in the field of biomedical applications are those with magnetic properties. Magnetic materials, especially iron oxides nanoparticles, are known since ancient times to have many spectacular properties, but in the last decade the properties that they possess at nanometric scale have been the starting point of great potential applications such as drug delivery, magnetic cell separation, tumor labeling and cell labeling. The most common forms of iron oxides, magnetite and maghemite (Fe_3O_4, γ-Fe_2O_3), are studied due to the outstanding properties they exhibit at nanometric scale (high specific surface area, superparamagnetism, etc.) [1–5]. The nanometric dimensions of these materials makes them ideal candidates for surface engineering and functionalization. Surface enhancement and functionalization facilitate the use of these nanomaterials in biomedical applications, for example, as contrast agents for magnetic resonance imaging (MRI) [6, 7], tissue-specific release of therapeutic agents, targeted drug delivery in tumor therapy [8], hyperthermia, cell labeling [9], magnetic cell sorting [10], and magnetic field assisted radionuclide therapy [11].

In the past few years, superparamagnetic iron oxide nanoparticles with controlled and enhanced surface chemistry properties have been used successfully as contrast agents for magnetic resonance imaging *in vivo* [12, 13]. The new direction of research aims to develop new compounds based on iron oxide nanoparticles for *in vivo* biomedical applications. Recent studies in the field of malignant tumors are focused on developing a new drug delivery systems based on iron oxide nanoparticles in order to avoid damaging the healthy cells around the tumor mass in the process of cancerous cell destruction. These types of nanosystems based on iron oxide nanoparticles have the ability to heat up,

delivering toxic amounts of thermal energy to tumors, or as chemotherapy and radiotherapy enhancement agents, where a controlled degree of tissue warming leads to an effective cell destruction [14, 15].

In agreement with Pisanic II et al. [16], magnetic nanoparticles could be used as tools in a wide variety of biomedical applications. On the other hand, Pisanic II et al. showed that failure to fully and properly evaluate nanostructures on an individual case-by-case basis may lead to lack of parameter control in *in vitro* experiments, as well as incorrect assumptions concerning their biocompatibility and biosafety of their *in vivo* use [16]. In order to improve the knowledge on cytotoxicity of iron oxide nanoparticles, we performed an *in vivo* toxicity study (48 h) by administration by intraperitoneal injection of γ-Fe_2O_3 dispersion at concentrations of 0.7 mL/kg, 1.7 mL/kg, and 3.7 mL/kg.

The aim of this study was to develop iron oxide nanoparticles by an adapted coprecipitation method [17–22] with controllable parameters and enhanced biocompatible properties for *in vivo* applications. Scanning electron microscopy (SEM) and transmission electron microscopy (TEM) studies have been conducted to obtain information about the size, structure, and morphology of IO-NPs. The biocompatibility of the iron oxide was evaluated using *in vitro* and *in vivo* assays, consisting in the quantification of HeLa cells viability and the histological evaluation of the nanoparticles effects on the male Brown Norway rat's tissues.

2. Experimental Section

2.1. Materials. Ferrous chloride tetrahydrate ($FeCl_2{\cdot}4H_2O$), ferric chloride hexahydrate ($FeCl_3{\cdot}6H_2O$), natrium hydroxide (NaOH), and chlorhidric acid (HCl) were purchased from Merck. Deionized water was used in the synthesis of nanoparticles and for rinsing the clusters.

2.2. Synthesis of Iron Oxide Ferrofluid. Iron oxide nanoparticles were prepared by coprecipitation [17–22]. Ferrous chloride tetrahydrate ($FeCl_2{\cdot}4H_2O$) in 2 M HCl and ferric chloride hexahydrate ($FeCl_3{\cdot}6H_2O$) were mixed at 100°C (Fe^{2+}/Fe^{3+} = 1/2). The mixture was dropped into 200 mL of NaOH (2 mol·L^{-1}) solution under vigorous stirring for about 30 min. The precipitate of magnetite (black precipitate immediately formed) was converted into γ-Fe_2O_3 particles by repeated treatment with HNO_3 (2 mol·L^{-1}) and $FeNO_3$ (0.3 mol·L^{-1}) solutions [23]. The acidic precipitate was isolated by decantation on a magnet, separated by centrifugation (6000 rpm), then washed in acetone, and dispersed in deionized water at pH = 2.5. The final ion concentration was 0.38 mol·L^{-1}. For biological investigations, the pH was adjusted to 7 using aqueous ammonia. The iron content of the suspensions was determined by redox-titration [23].

2.3. Characterization of Nanoparticles. The morphology of the obtained material was studied using a Quanta Inspect F scanning electron microscope (SEM), operating at 25 kV in vacuum. The elemental local analysis was performed using an energy dispersive spectroscopy (EDS) detector from EDAX. The operating conditions were an accelerating voltage between 2 and 25 keV (depending of the signal/noise ratio) for samples tilted at 25° in order to get the optimal take off angle (30°) allowing a dead time around 20–30% and a collecting time of 90–120 s. Transmission electron microscopy (TEM) images for these samples were recorded using a FEI Tecnai 12 equipped with a low dose digital camera from Gatan. The specimen for TEM imaging was prepared by ultramicrotomy in order to obtain a thin section of about 60 nm. The powder was embedded in an epoxy resin (polaron 612) before microtomy.

2.4. Cytotoxicity Assay. Quantification of cell viability was performed using propidium iodide (PI) and fluorescein diacetate (FdA). Briefly, $5{\times}10^4$ HeLa cells were seeded in each well of a 24-well plate and after 24 h, the monolayers were treated with a suspension of γ-Fe_2O_3 (200 μL) nanoparticles diluted 100 times. The effects on cellular viability were evaluated after 48 h by adding 100 μL PI (0.1 mg/mL) and 100 μL FdA (0.1 mg/mL) and fluorescence studies have been performed using Observer D1 Carl Zeiss microscope. The cell viability was established by the ratio between viable (green) and dead cells (red) counted on several microscopic fields [24].

The cell viability was determined by MTT colorimetric assay developed by Mosmann for *in vitro* cytotoxicity and cell proliferation measurements [25]. It was reported that the mitochondrial enzyme succinate-dehydrogenase within viable cells is able to cleave the MTT salt into formazan, a blue colored product. The amount of formazan produced, read on scanning multiwell spectrophotometer, is proportional to the number of viable cells present [25–27]. The cells were cultured in the medium (2.5 × 105 cells/mL) containing iron oxide nanoparticles for 12, 24, and 72 hours periods. Culture medium without iron oxide nanoparticles served as control in each experiment. The different final concentrations of the suspension of iron oxide nanoparticles were prepared in cell growth medium. Concentration ranges were 10, 20, and 30 μg/mL. The medium from each well was removed by aspiration, the cells were washed with 200 μL phosphate buffer saline solution (PBS)/well, and then 50 μL of 1 mg/mL MTT solution was added on each well. After 2 h of incubation, the MTT solution from each well was removed by aspiration. A volume of 50 μL isopropanol was added and the plate was shaken to dissolve formazan crystals. The optical density at 595 nm, for each well, was then determined using a Tecan multiplate reader (Tecan GENios, Grödic, Germany). The percent of viable cells cultured on the iron oxide nanoparticles was calculated in comparison with a control sample; the cells cultured on uncoated culture plastic vessels, being considered to have a viability of 100%.

2.5. Animals. Male Brown Norway rats (weighing ~300 ± 10 g) were purchased from the National Institute of Research and Development for Microbiology and Immunology "Cantacuzino," Bucharest. The rats were housed in an environment controlled for temperature (22 ± 2°C), light (12 h light/dark cycles), and humidity (60 ± 10%). The animals were maintained under specific pathogen free-conditions in accordance with NIH Guide for the Care and Use of laboratory Animals.

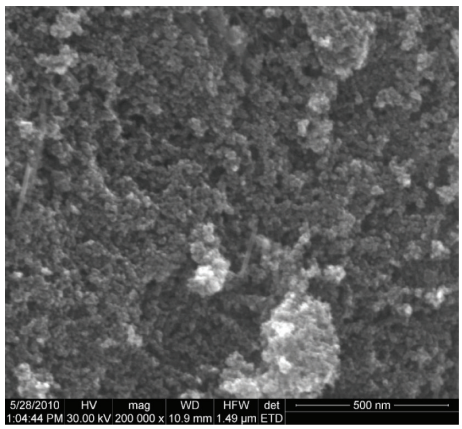

Figure 1: Scanning electron microscopy image of the synthesized iron oxide sample.

2.6. Histological Examination. For the analysis of iron oxide toxicity *in vivo*, the rats ($n = 4$ per group) were treated with normal saline and iron oxide (at concentrations of 0.7 mL/kg, 1.7 mL/kg, and 3.7 mL/kg) via intraperitoneal injection. The final ion concentration in iron oxide solution prepared by coprecipitations was 0.38 mol·L^{-1}. For histopathological examinations, selected organs (liver, kidney, lung and spleen) were removed from the rats and fixed in 10% formalin. The organs were prepared as paraffin-embedded glass slides stained with hematoxylin and eosin. The morphological changes were observed by microscopic examination [28].

3. Results and Discussion

SEM analysis was used to confirm the morphology of the synthesized iron oxide sample (Figure 1). The obtained results using scanning electron microscopy analysis clearly show that the IO-NPs have spherical shape. Detailed structural information and the growth direction of the maghemite, γ-Fe_2O_3, were obtained from TEM and HRTEM micrographs.

Figure 2(a) shows TEM picture of iron oxide nanoparticles (IO-NPs), clearly showing that the product is entirely composed of crystals with a relatively uniform, spherical morphology. Grain size distribution was determined by measuring the mean diameter, D, of about 500 particles on the micrographs (Figure 2(b)). TEM images indicate a very uniform size distribution of iron oxide nanoparticles. The average grain size of the monodisperse nanoparticles is 10 ± 0.3 nm. Figure 2(c) shows the selected area electron diffraction (SAED) pattern recorded from an area containing a large number of nanoparticles and the high-resolution TEM picture. The rings in the SAED pattern can be indexed as the (220), (311), (400), (422), (511), and (440) reflections of the cubic maghemite in agreement with the XRD results [29].

Despite the great potential of iron nanoparticles to be used for different industrial and medical applications, data about their toxicity are still scarce [30]. Bearing in mind that *in vitro* tests represent a first step of biomedical application investigation [31], we have studied the toxicity of the obtained nanoparticles on HeLa cells. It has been previously established that the optimum size of magnetic nanoparticles to promote an effective biodistribution is ranging from 10 to 100 nm [32]. From this point of view, the obtained nanoparticles meet this criterium, with a diameter of 10 nm. The results have shown that the obtained nanoparticles were not cytotoxic on the HeLa cells after 48 h exposure to a suspension of γ-Fe_2O_3 (200 μL) nanoparticles diluted 100 times (Figure 3(b)), as revealed by the absence of dead, red cells stained with propidium iodide (Figure 3). The low cytotoxicity of iron nanoparticles has been reported also by other authors and has been explained by the fact that the nanoparticles are not degraded within the timescale of the cellular assay (48 h) [33].

To examine the cytotoxicity of the iron oxide nanoparticles, the MTT assay was used. The HeLa cells were treated on/in a medium containing different concentrations (10, 20, and 30 μg/mL) of the suspension of iron oxide nanoparticles. Cell viability was determined at 12 h, 24 h, and 72 h after treatment and the test results are shown in Figure 4. We can see that the cell viability decreased when the concentration and time period increased. These results are in agreement with previous studies presented by Kouchesfehani et al. [34]. The toxic effect was taken into consideration when the survival rate was below 80%. The graph shows the mean +/− s.d. of normalized values on three independent experiments.

The *in vivo* toxicity study (48 h) was performed with γ-Fe_2O_3 dispersion administered by intraperitoneal injection at concentrations of 0.7 mL/kg, 1.7 mL/kg, and 3.7 mL/kg. The rats were observed after 48 h from each administration and their behavior was evaluated. All animals survived the administration of γ-Fe_2O_3 on all tested concentrations and did not show any sign of discomfort (lethargy, nausea, vomiting or diarrhea) during the whole duration of the experiment. The histopathological assessment of the selected tissues including liver, kidney, lung, and spleen was conducted.

At 48 h after the intraperitoneal injection no significant macroscopic histopathological changes were observed in the case of liver and kidney for all tested concentrations in the treated group compared with the control.

In Figure 5, the microscopic observations of the rat liver injected with different γ-Fe_2O_3 concentrations after 48 h are shown. The microscopic observations of the rat kidney injected with different γ-Fe_2O_3 concentrations after 48 h are presented in Figure 6.

Pathological sections of liver after injection with a 0.7 mL/kg dose of iron oxide nanoparticles (Figure 5(b)) show that the architecture of the liver was not affected by IO-NPs (0.7 mL/kg). Hepatocytes with discreet anisokaryosis, formation of chromocenters and nucleoli, and focal intrahepatocyte cholestasis (HE, 600x) were found in the liver of both the IO-NPs (0.7 mL/kg) treated and control groups (Figure 5(a)) with no significant difference between them. Greaves in histopathology of preclinical toxicity studies [35] showed that laboratory animals under conventional housing can undergo liver changes. On the other hand, he showed that granulomas are common spontaneous lesions in the liver. The liver changes may occur due to multiple causes such as drugs, bacterial, fungal, parasitic or viral infections, and liver or systemic disorders and are usually asymptomatic [36].

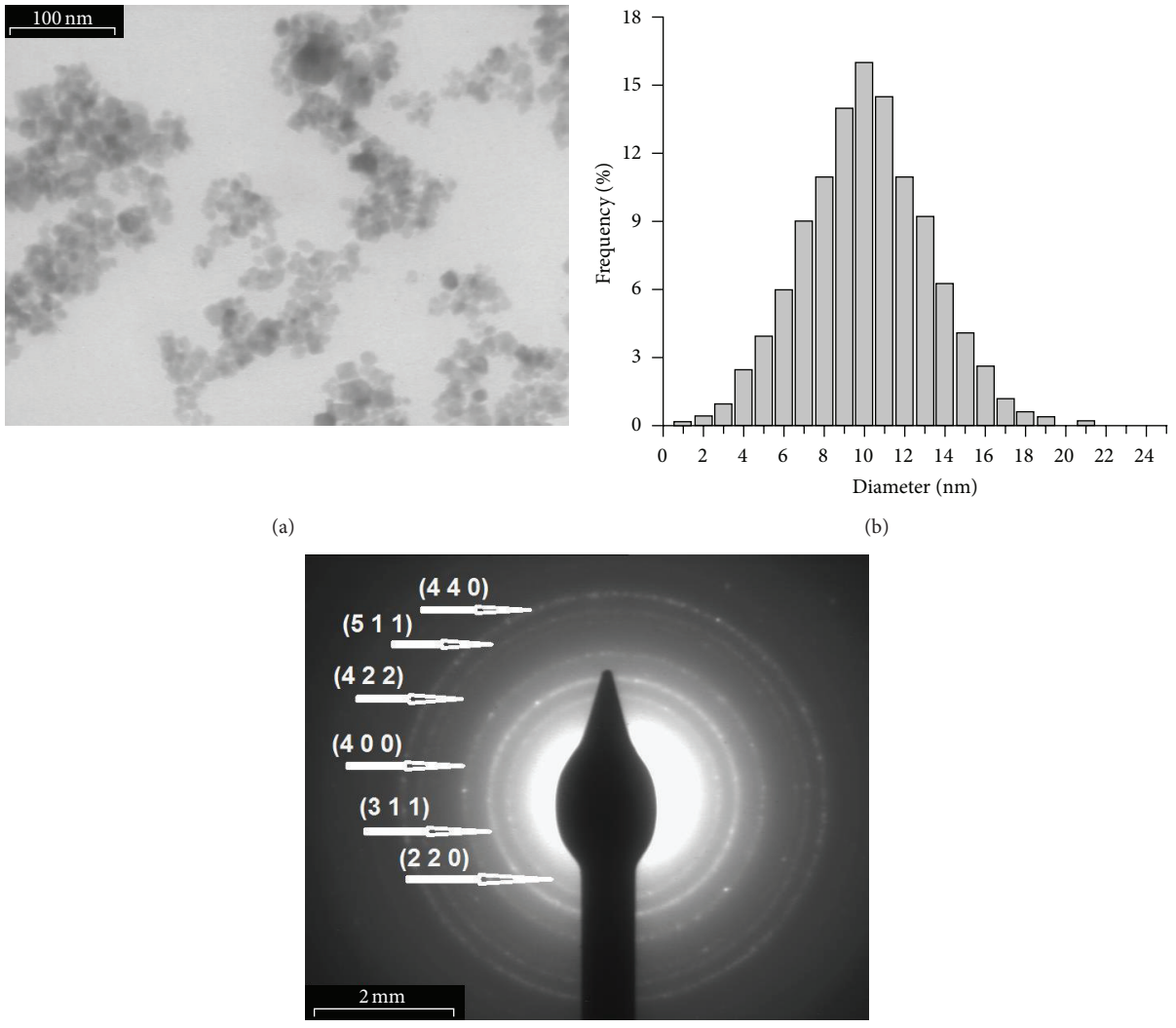

Figure 2: Bright field TEM picture showing a homogeneous distribution of iron oxide nanoparticles (a), size distribution of IO-NPs (b), and SAED pattern from a region including a large number of nanoparticles (c).

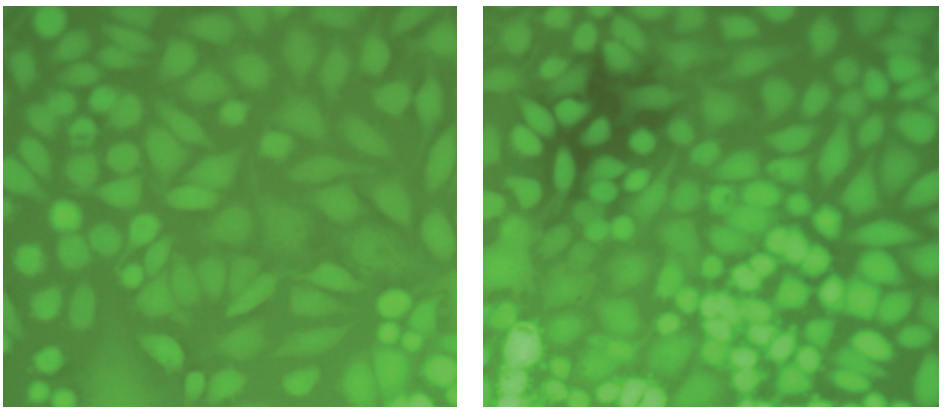

Figure 3: Inverted microscope image of HeLa cells after 48 h exposure to a suspension of γ-Fe_2O_3 (200 μL) nanoparticles diluted 100 times (b). Control cells cultured in free medium were run in parallel to the treated groups (a) (×200).

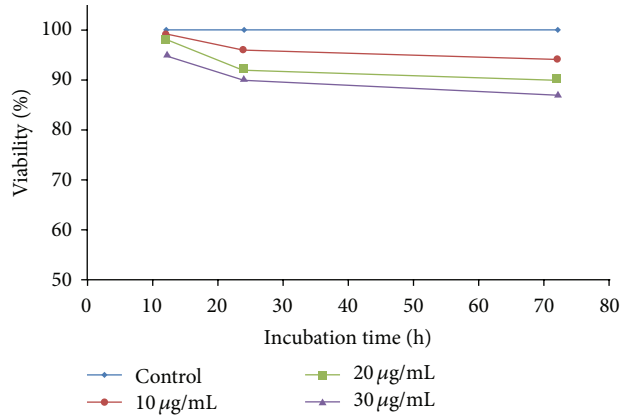

Figure 4: Effect of different concentrations of iron oxide nanoparticles on HeLa cells viability.

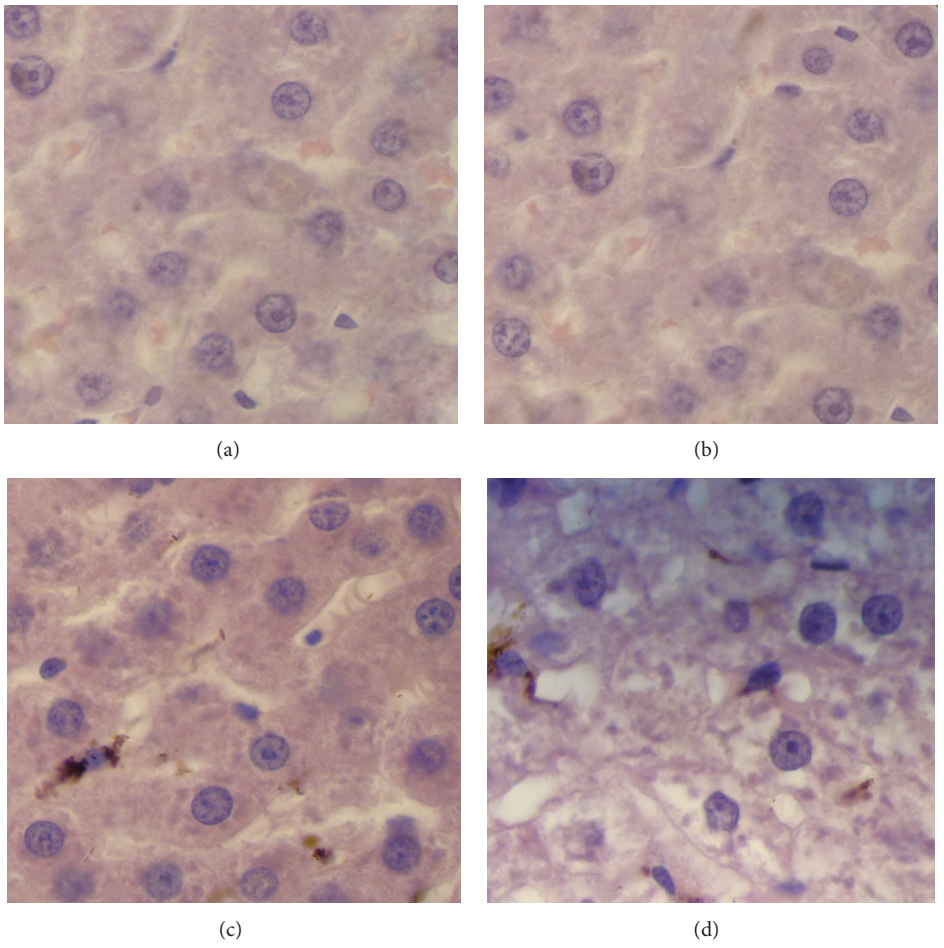

Figure 5: Light optical image of the liver after 48 h exposure to γ-Fe_2O_3 nanoparticles at concentrations of 0.7 mL/kg (b), 1.7 mL/kg (c), and 3.7 mL/kg (d). The reference sample is also presented (a).

The liver examination after the injection of 1.7 mL/kg dose of iron oxide nanoparticles (Figure 5(c)) indicates hepatocytes with moderate anisokaryosis, formation of chromocenters and nucleoli, and moderate granular cytoplasmic degeneration. The microgranular brown pigment deposits in Kupffer cells (HE, 600x) were also observed in the liver after injection with 1.7 mL/kg dose of iron oxide nanoparticles (Figure 5(c)). After injection with 3.7 mL/kg dose of iron oxide, nanoparticles (Figure 5(d)) were noticed hepatocytes with moderate anisokaryosis, formation of chromocenters and nucleoli. The granulovacuolar cytoplasmic degeneration and microgranular brown pigment deposits in Kupffer

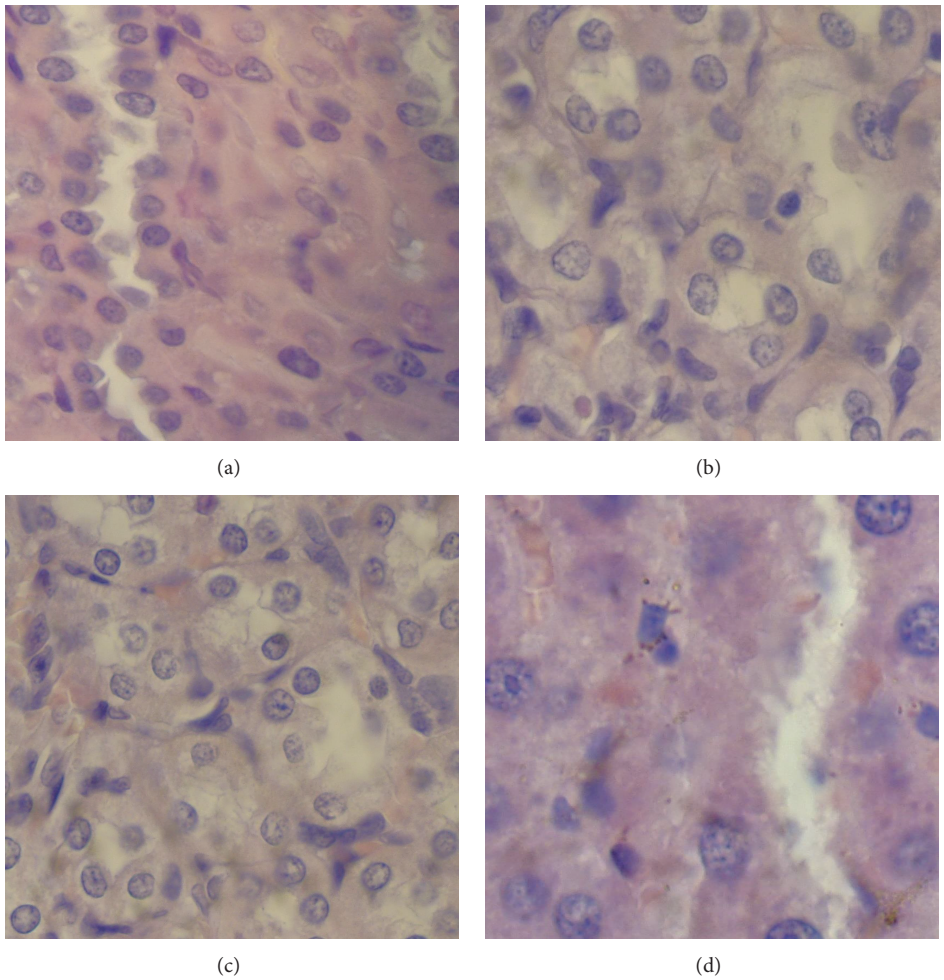

Figure 6: Light optical image of the kidney after 48 h exposure to γ-Fe_2O_3 nanoparticles at concentrations of 0.7 mL/kg (b), 1.7 mL/kg (c), and 3.7 mL/kg (d). The reference sample is also presented (a).

cells and hepatocytes (HE, 600x) were also distinguished (Figure 5(d)).

The pathological micrographs of kidneys in rats after injection with 0.7 mL/kg dose of iron oxide nanoparticles (Figure 6(b)) show that the kidney has preserved the architecture of the control specimen (Figure 6(a)) with no significant differences. The tubular cells with moderate anisokaryosis and anisochromia with formation of chromocenters and minimal granular cytoplasmic degeneration (HE, 600x) are also presented in Figure 6(b).

The specimen injected with a solution of 1.7 mL/kg iron oxide (Figure 6(c)) preserves the architecture, tubular cells with moderate anisokaryosis, and anisochromia with formation of chromocenters, moderate granulovacuolar cytoplasmic degeneration with focal clear cells, and moderate vascular congestion (HE, 400x). For the specimen injected with a solution containing 3.7 mL/kg iron oxide (Figure 6(d)) were observed tubular cells with pronounced architectural distortions, enlarged nuclei with irregular contours, formation of prominent nucleoli, marked granular cytoplasmic degeneration and discreet deposition of microgranular brown pigment in the renal interstitium (HE, 600x).

On the other hand, the microscopic observations of the rat lung and spleen injected with different γ-Fe_2O_3 concentrations after 48 h are presented in Figures 7 and 8.

In Figure 7, the pathological micrographs of lungs in rats after the injection with doses containing 0.7 mL/kg, 1.7 mL/kg, and 3.7 mL/kg of iron oxide nanoparticles and the pathological micrographs of the control specimen (Figure 7(a)) are presented. After injection with 0.7 mL/kg (Figure 6(b)) dose of iron oxide nanoparticles, the lung parenchyma of the rats shows preserved alveolar architecture with rare macrophages in the alveolar septa, discreet anisokaryosis, and anisochromia of type II pneumocytes with rare nucleoli. The focal ectatic capillaries in the alveolar septa are also presented. We can see that the pathological micrographs of lung in rats after injection with 0.7 mL/kg dose of iron oxide nanoparticles (Figure 7(b)) show that the lung has preserved the architecture of the control specimen (Figure 7(a)) with no significant differences. For the specimen injected with a solution containing 1.7 mL/kg iron oxide (Figure 7(c)), we observed that the lung parenchyma shows preserved alveolar architecture with rare macrophages in the alveolar septa, discreet anisokaryosis, and anisochromia of

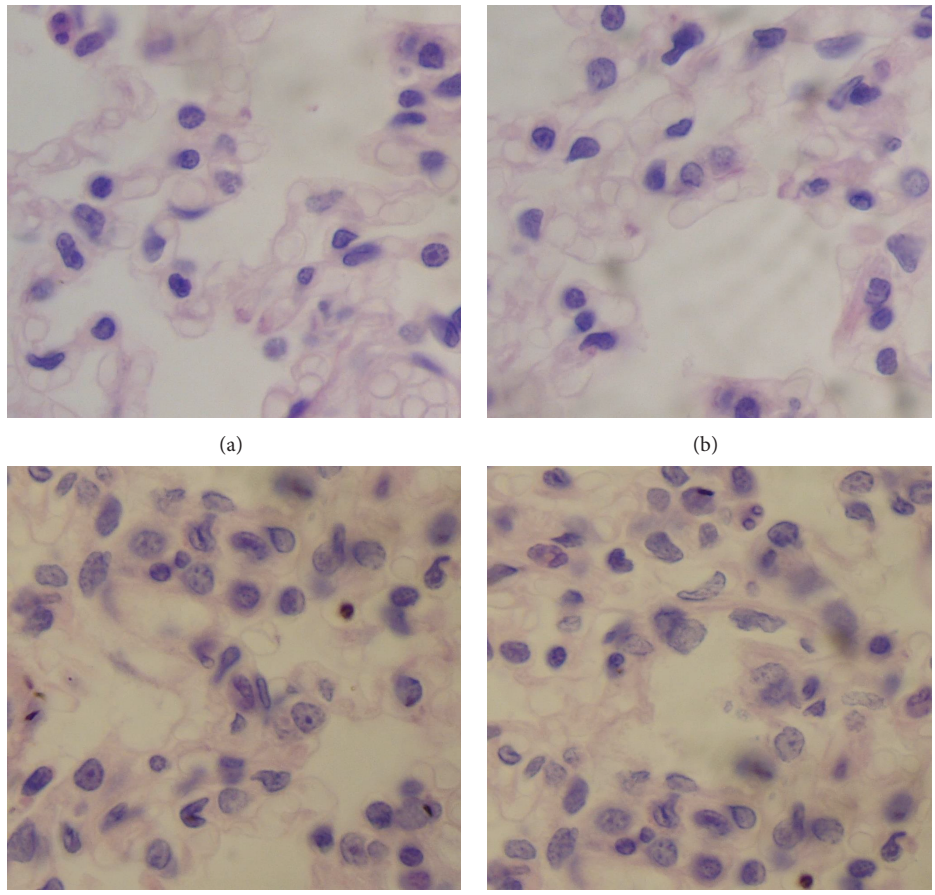

(a) (b) (c) (d)

Figure 7: Light optical image of the lung after 48 h exposure to γ-Fe_2O_3 nanoparticles at concentrations of 0.7 mL/kg (b), 1.7 mL/kg (c), and 3.7 mL/kg (d). The reference sample is also presented (a).

type II pneumocytes, with rare chromocenters and nucleoli. The focal ectatic capillaries in the alveolar septa are also presented. Lung parenchyma of the specimen injected with a solution of 3.7 mL/kg iron oxide (Figure 7(d)) shows preserved alveolar architecture with rare macrophages in the alveolar septa, discreet anisokaryosis, and anisochromia of type II pneumocytes, with rare chromocenters and nucleoli. In the lung parenchyma it is also observed focal ectatic capillaries in the alveolar septa.

Pathological sections of spleen after injection with a 0.7 mL/kg and 1.7 mL/kg dose of iron oxide nanoparticles (Figures 8(b)-8(c)) show that the architecture of the spleen was not affected by IO-NPs compared with the architecture of the control specimen (Figure 8(a)). After injection with 0.7 and 1.7 mL/kg dose of iron oxide nanoparticles, there were noticed splenic red pulp with discreet nuclear contour irregularities, discreet anisochromia with focal chromocenter formation, and rare nucleoli. After injection with a 3.7 mL/kg dose of iron oxide nanoparticles (Figure 8(d)), we observed the splenic red pulp with increased number of monocytes, with nuclear contour irregularities. The discreet anisochromia with focal chromocenter formation were also remarked in the splenic pulp after injection with a 3.7 mL/kg dose of iron oxide nanoparticles.

In the present study, we have established that the tested IO-NPs did not induce any morphological alterations such as an increase of granulomas or tissue damage to the liver and kidneys. The lack of morphological modifications to the liver and kidneys could be explained by the low amount of IO-NPs. For low concentrations of IO-NPs, the histopathological investigations performed after injection showed that the architecture of the liver and kidneys was not affected and no significant differences between the control groups and injected groups were observed. These results are in agreement with previous studies conducted by Wang et al. [32–37] which ascertained that the toxicity apparently depends on the type of nanoparticules and their concentration. Furthermore, Wang et al. showed that some metal nanoparticles as well as Zn nanoparticles are highly toxic in acute assessments. Previous studies realized by Dekkers et al. [38] showed that metal oxide nanoparticles, like some forms of silica (SiO_2), induce toxicity after subacute assessments.

Hillyer and Albrecht, in gastrointestinal persorption and tissue distribution of differently sized colloidal gold nanoparticles studies [39], show that the acute and subacute *in vivo* intraperitoneal administration studies are very important, allowing us to find the potential toxicological effects that iron oxide nanoparticles may have in key organs (gastrointestinal

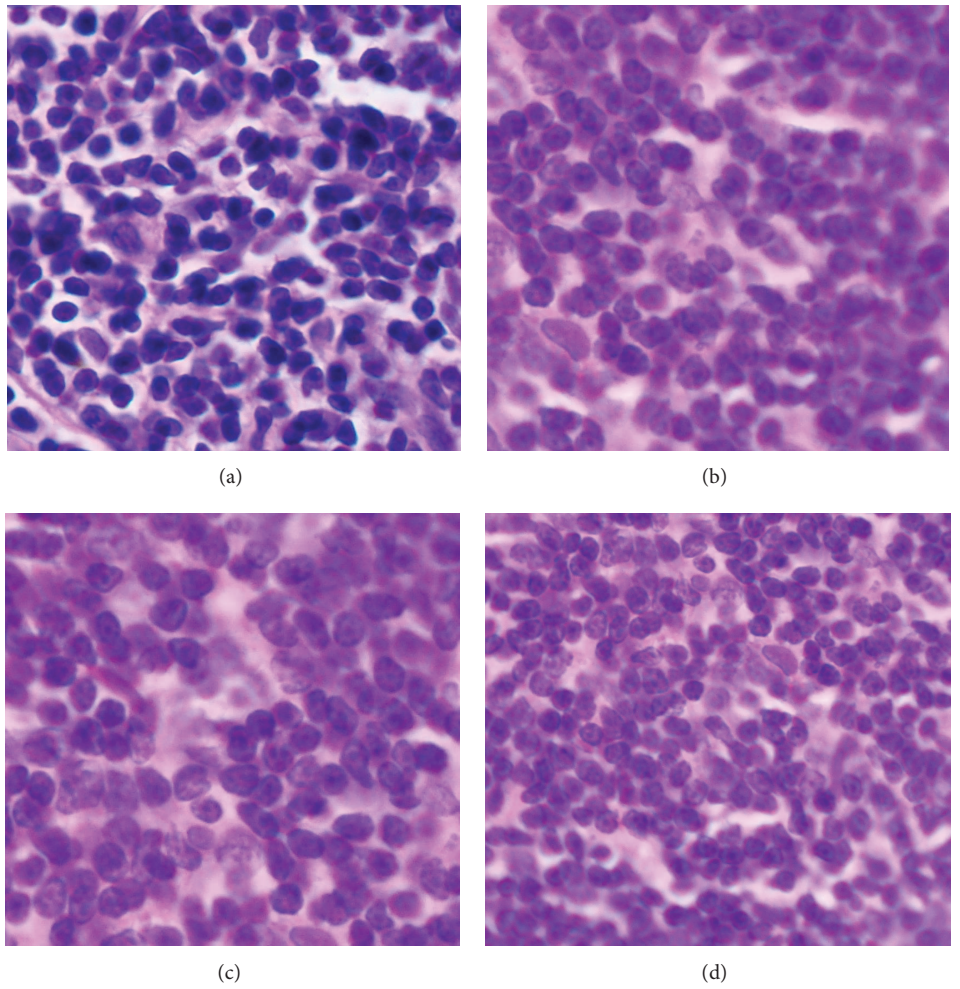

Figure 8: Light optical image of the spleen after 48 h exposure to γ-Fe_2O_3 nanoparticles at concentrations of 0.7 mL/kg (b), 1.7 mL/kg (c), and 3.7 mL/kg (d). The reference sample is also presented (a).

tract, liver, kidneys, and spleen) and the cardiovascular system. On the other hand, Kim et al. [40] showed that the study of the possibility of iron oxide nanoparticles to cross the intestinal barrier as well as their effects in blood serum, and the possible alteration to urinary parameters (potassium, sodium, and osmolality) is very important in order to understand the toxicity effects of these particles. Understanding the potential risks associated with exposure to iron oxide nanoparticles used for a great variety of medical applications is crucial. It is very important to design functionalize iron oxide nanoparticles that can be effectively internalized and which can meet the demands of a particular application without compromising on cellular toxicity.

4. Conclusions

The toxicity of the uniform, spherical obtained nanoparticles with 10 ± 0.3 nm in size has been investigated by *in vitro* and *in vivo* assays. At the tested concentrations, the nanoparticles proved to be not cytotoxic on HeLa cells and did not modify the rat's behavior or the histopathological aspect of liver, kidney, lung, and spleen tissues. Intraperitoneal injection of γ-Fe_2O_3 nanoparticles at several concentrations showed a normal macroscopic histopathological behavior of liver, kidney, lung, and spleen after 48 h for each concentration in the treated group compared with the control. Therefore, the preserved architecture of the control or slightly pathological changes of liver, kidney, lung, and spleen joint were induced by the low-dose of IO-NPs. The results of the present study suggested that the Fe_2O_3 nanoparticles could be used for future therapeutic alternative treatment strategies.

Acknowledgments

The financial and encouragement support provided by the Ministry of Educations of the Romania, Project no. C2-06 under program CEA-IFA, POSDRU/107/1.5/S/76813 (DocInvest), and by the scholarship of the French government via the cultural section of the French Embassy.

References

[1] S. Laurent, D. Forge, M. Port et al., "Magnetic iron oxide nanoparticles: synthesis, stabilization, vectorization, physic chemical characterizations and biological applications," *Chemical Reviews*, vol. 108, no. 6, pp. 2064–2110, 2008.

[2] S. Mornet, S. Vasseur, F. Grasset, and E. Duguet, "Magnetic nanoparticle design for medical diagnosis and therapy," *Journal of Materials Chemistry*, vol. 14, no. 14, pp. 2161–2175, 2004.

[3] A. M. Prodan, S. L. Iconaru, C. M. Chifiriuc et al., "Magnetic properties and biological activity evaluation of iron oxide nanoparticles," *Journal of Nanomaterials*, vol. 2013, Article ID 893970, 7 pages, 2013.

[4] E. Katz and I. Willner, "Integrated nanoparticle-biomolecule hybrid systems: synthesis, properties, and applications," *Angewandte Chemie*, vol. 43, no. 45, pp. 6042–6108, 2004.

[5] S. Laurent, S. Dutz, U. O. Häfeli, and M. Mahmoudi, "Magnetic fluid hyperthermia: focus on superparamagnetic iron oxide nanoparticles," *Advances in Colloid and Interface Science*, vol. 166, no. 1-2, pp. 8–23, 2011.

[6] C. H. Cunningham, T. Arai, P. C. Yang, M. V. McConnell, J. M. Pauly, and S. M. Conolly, "Positive contrast magnetic resonance imaging of cells labeled with magnetic nanoparticles," *Magnetic Resonance in Medicine*, vol. 53, no. 5, pp. 999–1005, 2005.

[7] S. A. Anderson, R. K. Rader, W. F. Westlin et al., "Magnetic resonance contrast enhancement of neovasculature with alpha(v)beta(3)-targeted nanoparticles," *Magnetic Resonance in Medicine*, vol. 44, no. 3, pp. 433–439, 2000.

[8] B. Polyak and G. Friedman, "Magnetic targeting for site-specific drug delivery: applications and clinical potential," *Expert Opinion on Drug Delivery*, vol. 6, no. 1, pp. 53–70, 2009.

[9] R. Weissleder, H.-C. Cheng, A. Bogdanova, and A. Bogdanov Jr., "Magnetically labeled cells can be detected by MR imaging," *Journal of Magnetic Resonance Imaging*, vol. 7, no. 1, pp. 258–263, 1997.

[10] E. A. Schellenberger, F. Reynolds, R. Weissleder, and L. Josephson, "Surface-functionalized nanoparticle library yields probes for apoptotic cells," *ChemBioChem*, vol. 5, no. 3, pp. 275–279, 2004.

[11] A. R. Jalilian, A. Panahifar, M. Mahmoudi, M. Akhlaghi, and A. Simchi, "Preparation and biological evaluation of [67Ga]-labeled- superparamagnetic nanoparticles in normal rats," *Radiochimica Acta*, vol. 97, no. 1, pp. 51–56, 2009.

[12] C. Corot, P. Robert, J.-M. Idée, and M. Port, "Recent advances in iron oxide nanocrystal technology for medical imaging," *Advanced Drug Delivery Reviews*, vol. 58, no. 14, pp. 1471–1504, 2006.

[13] C. Fan, W. Gao, Z. Chen et al., "Tumor selectivity of stealth multi-functionalized superparamagnetic iron oxide nanoparticles," *International Journal of Pharmaceutics*, vol. 404, no. 1-2, pp. 180–190, 2011.

[14] Q. A. Pankhurst, J. Connolly, S. K. Jones, and J. Dobson, "Applications of magnetic nanoparticles in biomedicine," *Journal of Physics D*, vol. 36, no. 13, pp. R167–R181, 2003.

[15] R. K. Gilchrist, W. D. Shorey, R. C. Hanselman, J. C. Parrott, and C. B. Taylor, "Selective inductive heating of lymph," *Annals of Surgery*, vol. 146, pp. 596–606, 1957.

[16] T. R. Pisanic II, J. D. Blackwell, V. I. Shubayev, R. R. Fiñones, and S. Jin, "Nanotoxicity of iron oxide nanoparticle internalization in growing neurons," *Biomaterials*, vol. 28, no. 16, pp. 2572–2581, 2007.

[17] R. Massart, "Magnetic fluids and process for obtaining them," US Patent 4329241, 1982.

[18] R. Massart, "Preparation of aqueous magnetic liquids in alkaline and acidic media," *IEEE Transactions on Magnetics*, vol. 17, pp. 1247–1248, 1981.

[19] R. Massart, J. Roger, and V. Cabuil, "New trends in chemistry of magnetic colloids: polar and non polar magnetic fluids, emulsions, capsules and vesicles," *Brazilian Journal of Physics*, vol. 25, no. 2, pp. 135–141, 1995.

[20] D. Predoi and C. Valsangiacom, "Thermal studies of magnetic spinel iron oxide in solution," *Journal of Optoelectronics and Advanced Materials*, vol. 9, no. 6, pp. 1797–1799, 2007.

[21] D. Zins, V. Cabuil, and R. Massart, "New aqueous magnetic fluids," *Journal of Molecular Liquids*, vol. 83, no. 1–3, pp. 217–232, 1999.

[22] D. Predoi, "A study on iron oxide nanoparticles coated with dextrin obtained by coprecipitation," *Digest Journal of Nanomaterials and Biostructures*, vol. 2, no. 1, pp. 169–173, 2007.

[23] S. Mornet, F. Grasset, J. Portier, and E. Duguet, "Maghemite@ silica nanoparticles for biological applications," *European Cells and Materials*, vol. 3S2, article 110, 2002.

[24] A. M. Grumezescu, E. Andronescu, A. Ficai, C. Bleotu, and M. C. Chifiriuc, "Chitin based biomaterial for antimicrobial therapy: fabrication, characterzation and in vitro profile based intercation with eukaryotic and prokaeryotic cells," *Biointerface Research in Applied Chemistry*, vol. 2, p. 446, 2012.

[25] T. Mosmann, "Rapid colorimetric assay for cellular growth and survival: application to proliferation and cytotoxicity assays," *Journal of Immunological Methods*, vol. 65, no. 1-2, pp. 55–63, 1983.

[26] F. Denizot and R. Lang, "Rapid colorimetric assay for cell growth and survival: modifications to the tetrazolium dye procedure giving improved sensitivity and reliability," *Journal of Immunological Methods*, vol. 89, no. 2, pp. 271–277, 1986.

[27] H. Wan, R. L. Williams, P. J. Doherty, and D. F. Williams, "The cytotoxicity evaluation of Kevlar and silicon carbide by MTT assay," *Journal of Materials Science*, vol. 5, no. 6-7, pp. 441–445, 1994.

[28] B. Su, S. L. Xiang, J. Su et al., "Diallyl disulfide increases histone acetylation and $P21^{WAF1}$ expression in human gastric cancer cells *in vivo* and *in vitro*," *Biochemical Pharmacology*, vol. 1, no. 7, pp. 1–10, 2012.

[29] C. S. Ciobanu, S. L. Iconaru, E. Gyorgy et al., "Biomedical properties and preparation of iron oxide-dextran nanostructures by MAPLE technique," *Chemistry Central Journal*, vol. 6, article 17, 2012.

[30] O. Krystofova, J. Sochor, O. Zitka et al., "Effect of magnetic nanoparticles on tobacco BY-2 cell suspension culture," *International Journal of Environmental Research and Public Health*, vol. 10, no. 1, pp. 47–71, 2013.

[31] L. L. C. Estevanato, J. R. Da Silva, A. M. Falqueiro et al., "Co-nanoencapsulation of magnetic nanoparticles and selol for breast tumor treatment: in vitro evaluation of cytotoxicity and magnetohyperthermia efficacy," *International Journal of Nanomedicine*, vol. 7, pp. 5287–5299, 2012.

[32] M. L. B. Carneiro, E. S. Nunes, R. C. A. Peixoto et al., "Free Rhodium (II) citrate and rhodium (II) citrate magnetic carriers as potential strategies for breast cancer therapy," *Journal of Nanobiotechnology*, vol. 9, article 11, 2011.

[33] L. Gu, R. H. Fang, M. J. Sailor, and J.-H. Park, "In vivo clearance and toxicity of monodisperse iron oxide nanocrystals," *ACS Nano*, vol. 6, no. 6, pp. 4947–4954, 2012.

[34] H. M. Kouchesfehani, S. rKiani, A. A. Rostami, and R. Fakheri, "Cytotoxic effect of iron oxide nanoparticles on mouse embryonic stem cells by MTT assay," *Iranian Journal of Toxicology*, vol. 7, no. 21, pp. 849–853, 2013.

[35] P. Greaves, "Liver and pancreas," in *Histopathology of Preclinical Toxicity Studies*, pp. 457–503, Academic Press, Elsevier, New York, NY, USA, 2007.

[36] A. Shiga, Y. Ota, Y. Ueda et al., "Study on the pathogenesis of foreign body granulomatous inflammation in the livers of sprague-dawley rats," *Journal of Toxicologic Pathology*, vol. 23, no. 4, pp. 253–260, 2010.

[37] B. Wang, W. Feng, M. Wang et al., "Acute toxicological impact of nano- and submicro-scaled zinc oxide powder on healthy adult mice," *Journal of Nanoparticle Research*, vol. 10, no. 2, pp. 263–276, 2008.

[38] S. Dekkers, P. Krystek, R. J. B. Peters et al., "Presence and risks of nanosilica in food products," *Nanotoxicology*, vol. 5, no. 3, pp. 393–405, 2011.

[39] J. F. Hillyer and R. M. Albrecht, "Gastrointestinal persorption and tissue distribution of differently sized colloidal gold nanoparticles," *Journal of Pharmaceutical Sciences*, vol. 90, no. 12, pp. 1927–1936, 2001.

[40] Y. S. Kim, J. S. Kim, H. S. Cho et al., "Twenty-eight-day oral toxicity, genotoxicity, and gender-related tissue distribution of silver nanoparticles in Sprague-Dawley rats," *Inhalation Toxicology*, vol. 20, no. 6, pp. 575–583, 2008.